

**Edge-State Selective Measurement of Dispersions in the Quantum Hall Regime**Henok Weldeyesus<sup>✉,\*</sup>, T. Patlatiuk, Q. Chen<sup>✉,†</sup>, C. P. Scheller<sup>✉</sup>, and D. M. Zumbühl<sup>✉,‡</sup>  
*Departement Physik, University of Basel, Klingelbergstrasse 82, CH-4056 Basel, Switzerland*A. Yacoby  
*Department of Physics, Harvard University, Cambridge, Massachusetts 02138, USA*L. N. Pfeiffer and K. W. West<sup>✉</sup>  
*Department of Electrical Engineering, Princeton University, Princeton, New Jersey 08544, USA* (Received 11 July 2025; accepted 3 November 2025; published 8 December 2025)

Edge states reflect the key physical properties yet are difficult to probe individually, particularly when several states are present at an edge. We present momentum resolved tunneling spectroscopy between a quantum well and a quantum wire to extract the dispersions of the quantum Hall edge states. Momentum and energy selective tunneling allows for separately addressing the different states even if they are spatially overlapping. This delivers the edge state velocities over broad ranges of magnetic field and density, in excellent agreement with a hard wall model. This technique provides a basis for future edge state selective spectroscopy on quantum materials.

DOI: [10.1103/h5ql-rnvh](https://doi.org/10.1103/h5ql-rnvh)

Edge states appearing on the boundary of topological insulators [1] and topological superconductors [2] are directly tied to the underlying bulk properties through bulk-boundary correspondence. To probe key properties such as the dispersions or the associated velocities of such edge states is, however, a more difficult task. Spectroscopic measurements such as angle resolved photoemission can play a crucial role in the investigation of the edge state properties and are often used to study surface and edge states of topological systems where the location of these states is exposed and accessible to optical measurements [3]. Consequently they are not applicable to quantum wells or buried structures in which many studies are performed.

Previous characterizations of quantum Hall edge state velocities in GaAs—one of the most studied material systems for the integer and fractional quantum Hall effects due to its ultrahigh mobility—relied on time-of-flight measurements of edge magnetoplasmons [4–7]. This technique was also applied to topological phases like the quantum anomalous Hall effect [8] and the quantum spin Hall effect [9], but it requires challenging ultrafast time-resolved setups. We note that the magnetoplasmon velocity is only vaguely related to the edge state velocity since it is a collective mode rather than a single edge state. Alternatively, quantum interferometry [10–15] was also employed. This

requires sufficiently small structures to keep the edge states coherent and is generally masked by competing Coulomb charging effects [16,17].

An important aspect of the investigation of edge states is the ability to selectively study their properties. Momentum-resolved tunneling spectroscopy presents a well established method to characterize the properties of electronic states in (partially) translation invariant systems [18,19]. Conservation of momentum automatically ensures individual addressability of the edge states if these have different momenta. Cleaved edge overgrowth devices [20] in various geometries [21,22] and gate-defined quantum wires [23] are most prominent. They were used to investigate 1D dispersions [24] and Luttinger liquid physics such as spin-charge separation [25,26] and charge fractionalization [27]. Quantum Hall edge states in such systems were also investigated with similar spectroscopy techniques, for example, edge state hybridization [28,29], edge confinement [30,31], edge state position evolution [29], and finally their wave functions [32].

In this Letter, we obtain the dispersions and velocities of edge states formed in a 2D electron gas (2DEG) in a cleaved edge overgrowth double quantum well structure. We probe the dispersion of a selected edge state by choosing its momentum with an in-plane magnetic field  $B_y$ . We pursue two approaches: at constant density, we probe the edge state evolution with bias voltage from small to large perpendicular magnetic field  $B_z$  which controls the Landau levels (LLs). Alternatively, we fix  $B_z$  and vary the density below a gate, following the lowest five LLs until their depletion. We compare the extracted velocities to a

\*Contact author: [henok.weldeyesus@unibas.ch](mailto:henok.weldeyesus@unibas.ch)

†Present address: Kavli Institute for Theoretical Sciences, University of Chinese Academy of Sciences, Beijing 100190, China.

‡Contact author: [dominik.zumbuhl@unibas.ch](mailto:dominik.zumbuhl@unibas.ch)

single-particle model using hard wall edge confinement and find good agreement with the measurements.

A diagram of the sample and measurement scheme is shown in Fig. 1(a). A 2DEG with an adjacent upper wire (UW) is tunnel-coupled to a lower wire (LW) directly below it. Surface gates  $g_7$ ,  $g_5$ , and  $g_3$  are used to deplete the 2DEG and UW, forming separate  $10\ \mu\text{m}$  sized regions, as shown. Current flows from a source ohmic contact (S) with the chemical potential  $\mu_S$  through the 2DEG and the UW, tunneling to the lower wire (thick wiggled arrow), propagating under  $g_5$ , and finally tunneling back to the upper system into the drain (D), which is grounded. We apply a source-drain voltage  $V_{SD}$  and a small AC voltage of  $6\ \mu\text{V}$  at low frequencies ( $\sim 17\ \text{Hz}$ ) to obtain the differential conductance  $g$  via standard lock-in measurements. In addition, we measure the voltage drop on the tunnel junctions, the source tunneling voltage  $V_{tS}$ , and the drain tunneling voltage  $V_{tD}$ , with two voltage probes A and B. This is needed because the voltage drop has a highly nonlinear dependence on the applied bias voltage  $V_{SD}$  and cannot be accounted for without a separate measurement. Here we will focus on the data from the drain junction. More details on the voltage measurement and complementary data from the source junction can be found in Supplemental Material [33].

We apply an in-plane magnetic field  $B_Y$  and an out-of-plane magnetic field  $B_Z$ , as indicated in Fig. 1(a). The spectroscopy field  $B_Y$  is parallel to the 2DEG and perpendicular to the plane spanned by the quantum wells and therefore provides a momentum kick  $\Delta k_x = eB_Y d/\hbar$  to tunneling electrons [24]. Here,  $e$  is the electron charge,  $d$  is the center-to-center distance between the quantum wells, and  $\hbar$  is the reduced Planck constant. This allows us to perform spectroscopy as a function of momentum by tuning  $B_Y$  and therefore provides the ability to selectively tunnel to only a single edge state even when many are present at that edge. Because of this momentum conserving tunneling process, this spectroscopy can also be performed at filling fractions corresponding to a conductive 2D bulk, where other techniques are not applicable.

The field  $B_Z$ , applied perpendicular to the 2DEG, induces the LLs. Throughout this Letter we only refer to the spin-degenerate LL since large magnetic fields are needed to resolve the spins [29]. The quench boundaries of the two-axis magnet are limiting application of large simultaneous magnetic fields. In addition to the Landau quantization,  $B_Z$  provides additional momentum when tunneling, related to the displacement in the  $y$  direction of the upper and lower systems, such that the total momentum shift becomes  $\Delta k_x = eB_Y d/\hbar + eB_Z \Delta y/\hbar$  [29,32]. This provides independent control of the momentum kick and the LLs. By applying a bias voltage, the dispersions in the upper and lower systems are shifted in the energy direction. The densities are assumed to be independent of the applied bias voltage [34]. The measured

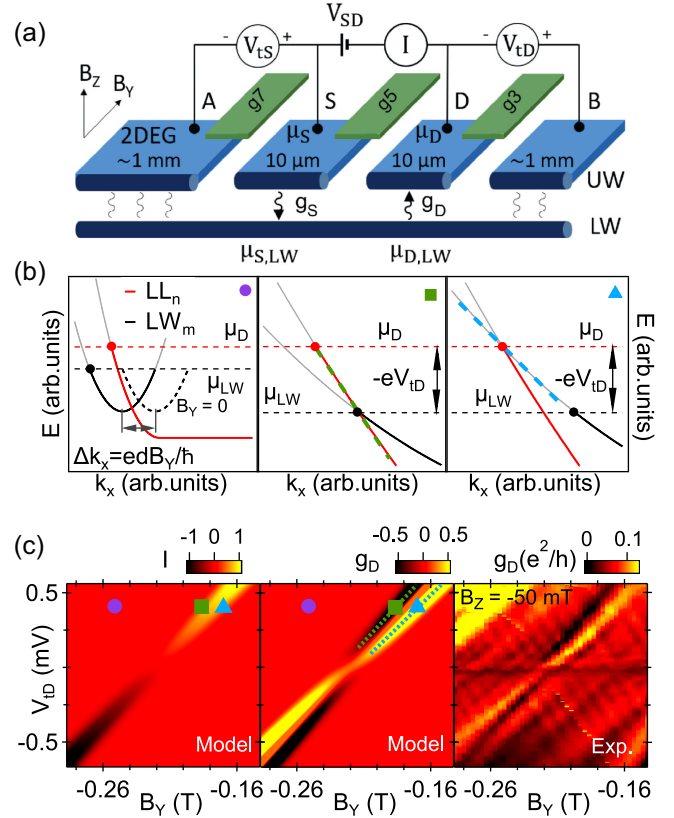


FIG. 1. Bias voltage tunneling spectroscopy. (a) Sample schematic for the velocity measurement. (b) Schematic of the dispersion for tunneling from a Landau level (LL) to a lower wire mode, at fixed tunnel junction voltage  $V_{tD}$  and varying magnetic fields from left to right when going through the panels. The left panel corresponds to a nonresonant condition. The second and third panels show a magnified view at two values of  $B_Y$ , corresponding to tracing out  $LL_n$  with the Fermi point of the  $LW_m$  and vice versa. (c) Simulated current and conductance (arb. units) (left and center panels) and corresponding conductance measurement, used to extract the velocities for a given LL and out-of-plane magnetic field  $B_Z$ . Each such measurement typically provides two mode velocities, a fast one and a slow one. The colored markers in the first two panels mark the positions of the situations depicted in (b).

tunnel current is enhanced when  $\Delta k_x$  and  $V_{SD}$  are adjusted such that filled states of one dispersion align with empty states in the other dispersion [35].

We now describe the extraction of the dispersion relations from the tunneling spectroscopy. We start by showing the calculated dispersion relation of an  $LL_n$  (red) and a lower wire mode  $LW_m$  (black) for three different values of the spectroscopy field at fixed voltage  $V_{tD}$  across the drain junction; see Fig. 1(b). The states above the chemical potential (horizontal dashed lines) are not populated with electrons and are shown in gray. The first panel shows the off-resonant case, where no matching is present (only filled states overlap each other close to the bottom of the LW dispersion). The second panel shows the matching

of the LW Fermi point with the filled states in the LL dispersion at a specific value of  $B_Y$ . This causes the current flow to turn on and remain on while empty, and filled states are overlapping at the intersection of the two dispersions. When the LL Fermi point starts to shift off the LW dispersion (right panel), the current shuts down.

The current turns on or off precisely when a Fermi point overlaps with the other dispersion, see the first panel in Fig. 1(c), which results in a corresponding peak or dip in the differential conductance, see Fig. 1(c). The peak and the dip indicate where one dispersion is mapped using the Fermi point of the other one, thus allowing us to separately extract each dispersion, i.e., the dispersions of the LL and LW modes. In the experiment, it is not always easy to identify such pairs of differential conductance peaks since other features such as finite size effects [36] or other modes can interfere. A relatively clean example is shown in Fig. 1(c) (third panel). The dispersions appear as lines here since the curvature is negligible given the applied bias is relatively small compared to the Fermi energy. The slope of these lines give the velocity of the corresponding modes,

$$v = \frac{1}{\hbar} \frac{dE}{dk_x} = \frac{1}{d} \frac{dV_{tD}}{dB_Y}, \quad (1)$$

where  $E$  and  $k_x$  are the energy and momenta of the states.

To study the evolution of LL velocities with the out-of-plane magnetic field we first identify the position of the tunneling resonances in the  $B_Y$ - $B_Z$  plane. These correspond to the matching of the LL and LW Fermi points at constant bias voltage and are shown in Fig. 2(a) for  $LL_0$  and  $LL_1$  tunneling to  $LW_2$ ; see Ref. [29] for the detailed identification of the various modes. Then,  $B_Z$  is fixed, and the bias spectroscopy, as shown in Fig. 1(c), is performed in a small range of spectroscopy field  $B_Y$  in the vicinity of the tunneling resonances. The values of  $B_Z$  where the spectroscopy is carried out are indicated by blue vertical lines in Fig. 2(a). These positions were chosen due to the increased contrast with respect to the background conductance.

The bias spectroscopy delivers always two velocities which need to be properly assigned to the LL or the LW. The LW mode is quite strongly confined and therefore relatively weakly affected by a moderate  $B_Z$  field, while the LLs increase their energy linearly with  $B_Z$  and the edge state velocities are reduced as the bulk LL approaches the Fermi level. We obtain a fast and a slow value from both LL branches [see Fig. 2(a)], delivering four different velocities. Then, we identify the two modes with the stronger  $B_Z$  dependence as  $LL_0$  and  $LL_1$ , plotted separately in Figs. 2(b) and 2(c), and the remaining two modes as two separate measurements of the  $LW_2$  velocities, see Fig. 2(d).

We find good agreement for the LL velocities with a hard wall model (see Supplemental Material) applicable here for the sharp cleaved edge potential; see the solid curves. The results here are in the same range as previous

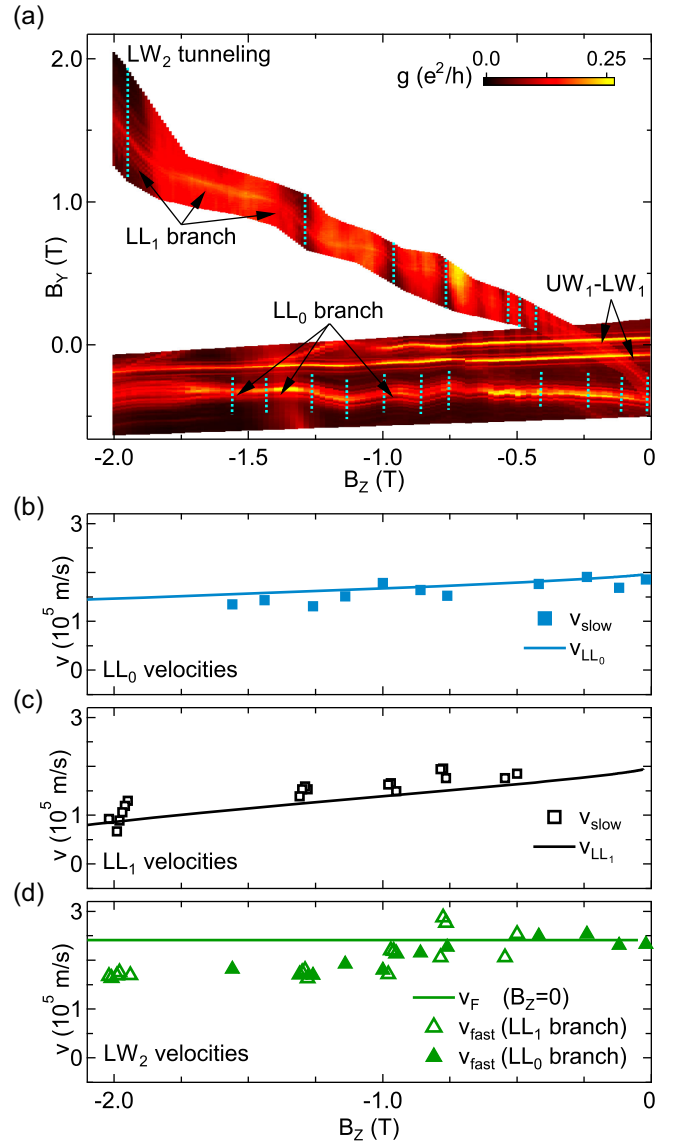


FIG. 2. Magnetic field evolution of velocities. (a) Zero bias tunnel map showing resonances as a function of out-of-plane field  $B_Z$  and spectroscopy field  $B_Y$ . Bias spectroscopy measurements are performed at each of the blue dashed vertical lines crossing both  $LL_0$  and  $LL_1$  (b) and  $LL_1$  (c) branches together with a hard wall model (solid lines). (d) The corresponding fast velocities together with the calculated  $LW_2$  Fermi velocity (solid green line), assumed to be  $B_Z$  independent.

measurements [10,11]. We note that 2DEG density is enhanced by about 50% at the edge compared to the measured bulk density. This is due to the presence of the ionized donors on the cleaved edge side as previously reported [29,32]. The  $LW_2$  velocities turn out to be the fastest ones extracted here, and we see good agreement between the values from both LL branches. Further, they also agree well with the calculated Fermi velocity (solid green line) from the densities in these modes as obtained

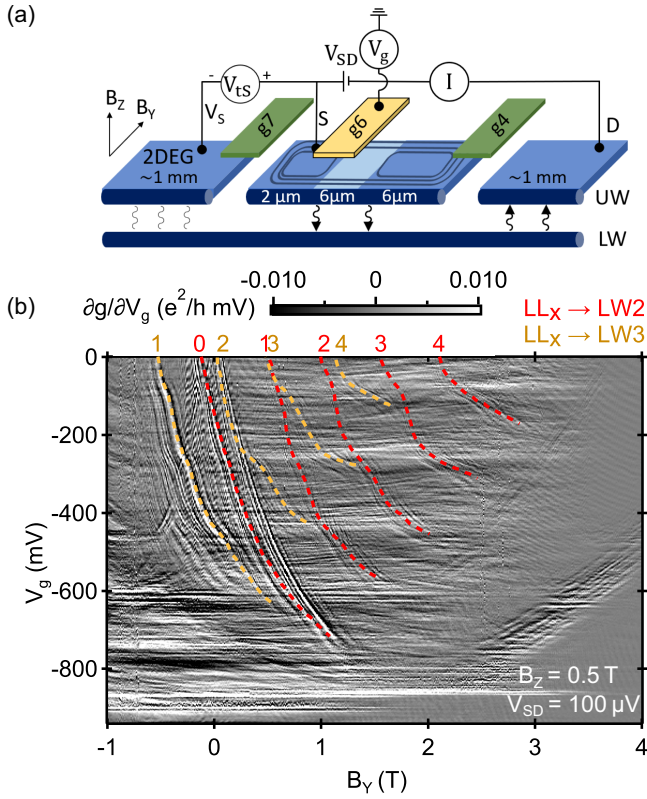


FIG. 3. Density dependent spectroscopy. (a) Setup for the density dependent measurement. The conductance is measured on the source junction, on which a gate (g6) is used to locally change the density. (b) Zero bias tunnel map showing resonances as a function of spectroscopy field  $B_Y$  and gate voltage  $V_{g6}$  performed at  $B_Z = 0.5$  T. The red and orange curves correspond to tunneling between the LL and the  $LW_2$  or  $LW_3$ , respectively.

from low-B spectroscopy [29]. As  $B_Z$  is increased above  $\sim 1$  T, a slight reduction of the measured  $LW_2$  velocities is observed, consistent with incipient magnetic depopulation of the mode (not included in the model).

We also perform a second experiment at constant bias voltage and instead extract the velocities at constant  $B_Z$  as a function of density controlled with a gate voltage. As before, we observe increased conductance when matching the Fermi points of the LW modes with the LL dispersion, or vice versa. Instead of shifting the dispersions in energy, the reduction in the density of both the 2DEG and the wire modes causes a change in their Fermi wave number  $k_F$ , which leads to a shift of the resonance position in the  $V_g$ - $B_Y$  plane (see Supplemental Material). The measurement configuration is shown in Fig. 3(a), and the gate voltage  $V_g$  is applied to gate g6. The adjacent gates g7 and g4 are defining the source tunnel junction by depleting the 2DEG and upper wire. We fix the out-of-plane field  $B_Z$  at 0.5 T and then record the tunneling conductance as a function of spectroscopy field  $B_Y$  and top-gate voltage  $V_g$ . In principle this experiment can be performed at zero bias, but a fixed, small bias voltage of  $V_{SD} \sim 100$   $\mu$ V is applied to avoid the

zero-bias anomaly [37,38]. This simplified measurement scheme avoids the voltage measurement of Fig. 1(a) since the position of the resonance does not strongly depend on bias voltage.

The measurement is shown in Fig. 3(b), where a derivative with respect to gate voltage was taken to remove a smooth background stemming from the ungated section of the source region. Two sets of resonances are shown in red and yellow, denoting tunneling to  $LW_2$  and  $LW_3$ , respectively. The mode assignments are apparent from a larger  $B_Z$ - $B_Y$  map shown in Ref. [29], and the mode densities are extracted in Supplemental Material [33]. These resonances are only visible up to certain gate voltages, where they vanish, marking the depletion of that LL and the corresponding edge state. In addition to the marked resonances, replicas due to finite size effects of the 6  $\mu$ m gate are seen to follow in parallel [36]. Where a LL crosses a wire mode in the upper system, hybridization gaps are observed [32], which is discussed in more detail in Supplemental Material [33].

In the gate dependent measurement no direct energy scale is acquired due to the fixed bias voltage. Therefore, a different approach has to be considered. The energy of an electron at the Fermi level depends on the density which is varied by the gate voltage, such that  $E = E[n(V_g)]$ . The velocity can then be expressed as

$$v = \frac{1}{\hbar} \frac{\partial E}{\partial k_x} = \frac{1}{e d} \frac{\partial E}{\partial n} \frac{\partial n}{\partial V_g} \frac{\partial V_g}{\partial B_Y}. \quad (2)$$

The three derivatives are  $\partial E/\partial n = D(E)^{-1}$ , the inverse density of states (DOS),  $\partial n/\partial V_g = \alpha$  the density lever arm, and  $\partial V_g/\partial B_Y$  is the slope of the resonances as identified in Fig. 3(a). Here, we have used the momentum kick  $\Delta k_x = e B_Y d/\hbar$  and the relation  $n(V_g) = \alpha(V_g - V_{th})$ , where  $V_{th}$  is the threshold voltage for the 2DEG depletion.

In the presence of an out-of-plane magnetic field the constant DOS  $D_{2D}$  is transformed into the comb of LLs. To perform the analysis we assume the constant DOS. This approximation becomes progressively worse as  $B_Z$  is increased but, as we will see, still yields good results at the present out-of-plane field of 0.5 T. The resulting velocities are displayed in Fig. 4(b) as a function of gate voltage. Two observations can be made. The velocity of the lower lying LLs is larger compared to higher LLs, and for all LL the velocity decreases as the density is lowered and the LL is depleted. Both observations are consistent with a simple LL edge state picture as shown in Fig. 4(a). The LLs closer to the edge bend up more strongly, obtaining a larger velocity. Further, we observe an oscillatory effect on the velocities, which can be attributed to the simplified DOS approximation.

Further we can convert the gate voltage into an energy by integrating  $\partial E/\partial V_g = -\alpha/D(E)$ . With this, we can transform the extracted resonances of the form  $V_g(B_Y)$  to the LL

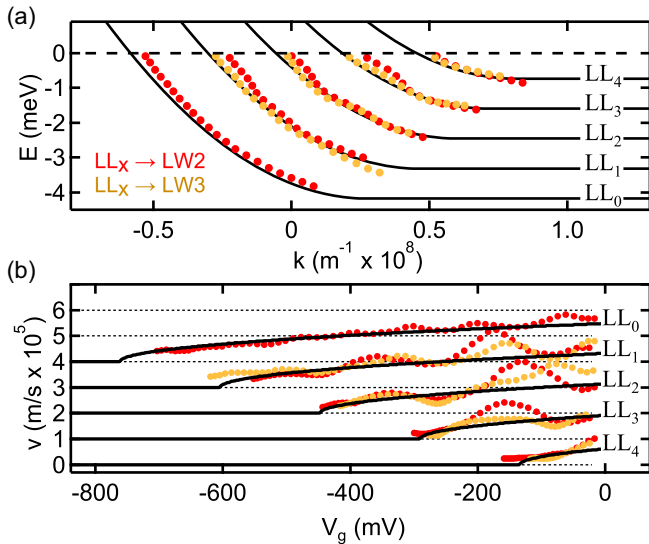


FIG. 4. Dispersions and velocities. (a) Dispersion of LLs extracted from the resonances in Fig. 3(a), with solid curves corresponding to theory for hard wall edge confinement. Marker colors are the same as in Fig. 3(a) and indicate tunneling from  $LW_2$  (red) and  $LW_3$  (orange). (b) Extracted velocities as a function of gate voltage for the resonances shown in Fig. 3(a). For clarity, each LL is offset by  $10^5$  m/s from the one plotted below.  $LL_4$  has no offset. Solid curves are the derivative  $\partial E / \partial k_x$  of the theory curves shown in (a).

dispersion relation,  $E(k_x)$ , shown in Fig. 4(a) for the first five spin degenerate LLs. Additionally, we show the calculated dispersions (solid curves) modeled from Ref. [32] for edge states of a LL confined by a hard wall. The effect of the constant DOS used to extract the dispersions is much smaller here than for the velocities because these depend on the derivative of the dispersions.

In conclusion, we have employed two versions of momentum resolved tunneling to extract dispersions and velocities of edge states in the integer quantum Hall effect. First, using a small bias voltage we extracted the velocities over a large range of perpendicular magnetic fields. We observe a reduction of the velocities as the magnetic field is increased, in agreement with a simple hard wall model. Second, we performed spectroscopy while varying the density, thereby obtaining the evolution of the velocities at a fixed  $B_z$ . In this way, we can directly access the edge state dispersions, and can even study the edge states of the same filling factors at many combinations of out-of-plane field and density.

In the future, this method can be applied to different material systems, such as HgTe, where intricate topological phases can occur [39]. But even in the current device, spin split states at higher fields and edge reconstruction effects [29] could be studied. Further, these methods can help to shed more light on the complexities of the edge structure of fractional quantum Hall edge states [40,41] since momentum resolved tunneling can give access to these

complicated, sometimes even counter propagating edge modes. Similarly, one could potentially also discriminate between different  $5/2$  candidate states [42]. As density is lowered, the ratio of kinetic to potential energy decreases, which can give rise to correlated phases [43,44] that may also be observed in their edge structure [45].

*Acknowledgments*—We thank G. Barak for providing access to this sample. This research was funded by Swiss SNSF (Grants No. 179024 and No. 215757), the NCCR SPIN of the Swiss SNSF, and the EU H2020 European Microkelvin Platform EMP (Grant No. 824109). C. P. S. acknowledges support by the Georg H. Endress Foundation.

*Data availability*—The data that support the findings of this article are openly available [46].

- [1] M. Z. Hasan and C. L. Kane, Colloquium: Topological insulators, *Rev. Mod. Phys.* **82**, 3045 (2010).
- [2] X.-L. Qi and S.-C. Zhang, Topological insulators and superconductors, *Rev. Mod. Phys.* **83**, 1057 (2011).
- [3] S. Lisi *et al.*, Observation of flat bands in twisted bilayer graphene, *Nat. Phys.* **17**, 189 (2020).
- [4] H. Kamata, T. Ota, K. Muraki, and T. Fujisawa, Voltage-controlled group velocity of edge magnetoplasmon in the quantum hall regime, *Phys. Rev. B* **81**, 085329 (2010).
- [5] N. Kumada, H. Kamata, and T. Fujisawa, Edge magnetoplasmon transport in gated and ungated quantum hall systems, *Phys. Rev. B* **84**, 045314 (2011).
- [6] M. Kataoka, N. Johnson, C. Emary, P. See, J. P. Griffiths, G. A. C. Jones, I. Farrer, D. A. Ritchie, M. Pepper, and T. J. B. M. Janssen, Time-of-flight measurements of single-electron wave packets in quantum hall edge states, *Phys. Rev. Lett.* **116**, 126803 (2016).
- [7] C. Lin, M. Hashisaka, T. Akiho, K. Muraki, and T. Fujisawa, Quantized charge fractionalization at quantum hall Y junctions in the disorder dominated regime, *Nat. Commun.* **12**, 131 (2021).
- [8] L. A. Martinez, G. Qiu, P. Deng, P. Zhang, K. G. Ray, L. Tai, M.-T. Wei, H. He, K. L. Wang, J. L. DuBois, and D.-X. Qu, Edge magnetoplasmon dispersion and time-resolved plasmon transport in a quantum anomalous hall insulator, *Phys. Rev. Res.* **6**, 013081 (2024).
- [9] A. Gourmelon, E. Frigerio, H. Kamata, L. Lunczer, A. Denis, P. Morfin, M. Rosticher, J.-M. Berroir, G. Fève, B. Plaçais, H. Buhmann, L. W. Molenkamp, and E. Bocquillon, Velocity and confinement of edge plasmons in HgTe-based two-dimensional topological insulators, *Phys. Rev. B* **108**, 035405 (2023).
- [10] D. T. McClure, Y. Zhang, B. Rosenow, E. M. Levenson-Falk, C. M. Marcus, L. N. Pfeiffer, and K. W. West, Edge-state velocity and coherence in a quantum hall Fabry-Pérot interferometer, *Phys. Rev. Lett.* **103**, 206806 (2009).
- [11] I. Gurman, R. Sabo, M. Heiblum, V. Umansky, and D. Mahalu, Dephasing of an electronic two-path interferometer, *Phys. Rev. B* **93**, 121412(R) (2016).

- [12] Y. Ji, Y. Chung, D. Sprinzak, M. Heiblum, D. Mahalu, and H. Shtrikman, An electronic Mach–Zehnder interferometer, *Nature (London)* **422**, 415 (2003).
- [13] I. Neder, M. Heiblum, Y. Levinson, D. Mahalu, and V. Umansky, Unexpected behavior in a two-path electron interferometer, *Phys. Rev. Lett.* **96**, 016804 (2006).
- [14] J. Nakamura, S. Liang, G. C. Gardner, and M. J. Manfra, Direct observation of anyonic braiding statistics, *Nat. Phys.* **16**, 931 (2020).
- [15] M. P. Rössli, M. Hug, G. Nicolí, P. Märki, C. Reichl, B. Rosenow, W. Wegscheider, K. Ensslin, and T. Ihn, Fractional Coulomb blockade for quasi-particle tunneling between edge channels, *Sci. Adv.* **7**, eabf5547 (2021).
- [16] B. I. Halperin, A. Stern, I. Neder, and B. Rosenow, Theory of the Fabry-Pérot quantum hall interferometer, *Phys. Rev. B* **83**, 155440 (2011).
- [17] J. Nakamura, S. Fallahi, H. Sahasrabudhe, R. Rahman, S. Liang, G. C. Gardner, and M. J. Manfra, Aharonov-Bohm interference of fractional quantum hall edge modes, *Nat. Phys.* **15**, 563 (2019).
- [18] R. K. Hayden, D. K. Maude, L. Eaves, E. C. Valadares, M. Henini, F. W. Sheard, O. H. Hughes, J. C. Portal, and L. Cury, Probing the hole dispersion curves of a quantum well using resonant magnetotunneling spectroscopy, *Phys. Rev. Lett.* **66**, 1749 (1991).
- [19] R. K. Hayden, E. C. Valadares, M. Henini, L. Eaves, D. K. Maude, and J. C. Portal, Anisotropy of the confined hole states in a (311)A AlAs/GaAs/AlAs quantum-well system: Evidence for a camel’s-back band structure, *Phys. Rev. B* **46**, 15586 (1992).
- [20] L. Pfeiffer, H. Störmer, K. Baldwin, K. West, A. Goñi, A. Pinczuk, R. Ashoori, M. Dignam, and W. Wegscheider, Cleaved edge overgrowth for quantum wire fabrication, *J. Cryst. Growth* **127**, 849 (1993).
- [21] G. Schedelbeck, W. Wegscheider, M. Bichler, and G. Abstreiter, Coupled quantum dots fabricated by cleaved edge overgrowth: From artificial atoms to molecules, *Science* **278**, 1792 (1997).
- [22] M. Grayson, C. Kurdak, D. Tsui, S. Parihar, S. Lyon, and M. Shayegan, Novel cleaved edge overgrowth structures for tunneling into one- and two-dimensional electron systems, *Solid State Electron.* **40**, 233 (1996).
- [23] B. Kardynał, C. H. W. Barnes, E. H. Linfield, D. A. Ritchie, J. T. Nicholls, K. M. Brown, G. A. C. Jones, and M. Pepper, Magnetotunneling spectroscopy of one-dimensional wires, *Phys. Rev. B* **55**, R1966 (1997).
- [24] O. M. Auslaender, A. Yacoby, R. De Picciotto, K. W. Baldwin, L. N. Pfeiffer, and K. W. West, Tunneling spectroscopy of the elementary excitations in a one-dimensional wire, *Science* **295**, 825 (2002).
- [25] O. M. Auslaender, H. Steinberg, A. Yacoby, Y. Tserkovnyak, B. I. Halperin, K. W. Baldwin, L. N. Pfeiffer, and K. W. West, Spin-charge separation and localization in one dimension, *Science* **308**, 88 (2005).
- [26] Y. Jompol, C. J. B. Ford, J. P. Griffiths, I. Farrer, G. A. C. Jones, D. Anderson, D. A. Ritchie, T. W. Silk, and A. J. Schofield, Probing spin-charge separation in a Tomonaga-Luttinger liquid, *Science* **325**, 597 (2009).
- [27] H. Steinberg, G. Barak, A. Yacoby, L. N. Pfeiffer, K. W. West, B. I. Halperin, and K. Le Hur, Charge fractionalization in quantum wires, *Nat. Phys.* **4**, 116 (2007).
- [28] W. Kang, H. L. Stormer, L. N. Pfeiffer, K. W. Baldwin, and K. W. West, Tunneling between the edges of two lateral quantum Hall systems, *Nature (London)* **403**, 59 (2000).
- [29] T. Patlatiuk, C. P. Scheller, D. Hill, Y. Tserkovnyak, G. Barak, A. Yacoby, L. N. Pfeiffer, K. W. West, and D. M. Zumbühl, Evolution of the quantum hall bulk spectrum into chiral edge states, *Nat. Commun.* **9**, 3692 (2018).
- [30] M. Huber, M. Grayson, M. Rother, R. Deutschmann, W. Biberacher, W. Wegscheider, M. Bichler, and G. Abstreiter, Tunneling in the quantum hall regime between orthogonal quantum wells, *Physica (Amsterdam)* **12E**, 125 (2002).
- [31] M. Huber, M. Grayson, M. Rother, W. Biberacher, W. Wegscheider, and G. Abstreiter, Structure of a single sharp quantum hall edge probed by momentum-resolved tunneling, *Phys. Rev. Lett.* **94**, 016805 (2005).
- [32] T. Patlatiuk, C. P. Scheller, D. Hill, Y. Tserkovnyak, J. C. Egues, G. Barak, A. Yacoby, L. N. Pfeiffer, K. W. West, and D. M. Zumbühl, Edge-state wave functions from momentum-conserving tunneling spectroscopy, *Phys. Rev. Lett.* **125**, 087701 (2020).
- [33] See Supplemental Material at <http://link.aps.org/supplemental/10.1103/h5ql-rmvh> for finite size effects, voltage corrections, complementary data, mode-hybridization, and numerical models.
- [34] D. Boese, M. Governale, A. Rosch, and U. Zülicke, Mesoscopic effects in tunneling between parallel quantum wires, *Phys. Rev. B* **64**, 085315 (2001).
- [35] O. M. Auslaender, A. Yacoby, R. de Picciotto, K. W. Baldwin, L. N. Pfeiffer, and K. W. West, Experimental evidence for resonant tunneling in a Luttinger liquid, *Phys. Rev. Lett.* **84**, 1764 (2000).
- [36] Y. Tserkovnyak, B. I. Halperin, O. M. Auslaender, and A. Yacoby, Finite-size effects in tunneling between parallel quantum wires, *Phys. Rev. Lett.* **89**, 136805 (2002).
- [37] Y. Tserkovnyak, B. I. Halperin, O. M. Auslaender, and A. Yacoby, Interference and zero-bias anomaly in tunneling between Luttinger-liquid wires, *Phys. Rev. B* **68**, 125312 (2003).
- [38] C. P. Scheller, T.-M. Liu, G. Barak, A. Yacoby, L. N. Pfeiffer, K. W. West, and D. M. Zumbühl, Possible evidence for helical nuclear spin order in GaAs quantum wires, *Phys. Rev. Lett.* **112**, 066801 (2014).
- [39] M. König, S. Wiedmann, C. Brune, A. Roth, H. Buhmann, L. W. Molenkamp, X.-L. Qi, and S.-C. Zhang, Quantum spin hall insulator state in HgTe quantum wells, *Science* **318**, 766 (2007).
- [40] A. H. MacDonald, Edge states in the fractional-quantum-Hall-effect regime, *Phys. Rev. Lett.* **64**, 220 (1990).
- [41] R. Sabo, I. Gurman, A. Rosenblatt, F. Lafont, D. Banitt, J. Park, M. Heiblum, Y. Gefen, V. Umansky, and D. Mahalu, Edge reconstruction in fractional quantum Hall states, *Nat. Phys.* **13**, 491 (2017).
- [42] S. Manna, A. Das, M. Goldstein, and Y. Gefen, Full classification of transport on an equilibrated  $5/2$  edge via shot noise, *Phys. Rev. Lett.* **132**, 136502 (2024).

- [43] H. M. Yoo, K. W. Baldwin, K. West, L. Pfeiffer, and R. C. Ashoori, Spin phase diagram of the interacting quantum hall liquid, *Nat. Phys.* **16**, 1022 (2020).
- [44] W. Pan, A. Serafin, J.S. Xia, L. Yin, N.S. Sullivan, K. W. Baldwin, K. W. West, L. N. Pfeiffer, and D. C. Tsui, Competing quantum hall phases in the second landau level in the low-density limit, *Phys. Rev. B* **89**, 241302(R) (2014).
- [45] F. Lafont, A. Rosenblatt, M. Heiblum, and V. Umansky, Counter-propagating charge transport in the quantum hall effect regime, *Science* **363**, 54 (2019).
- [46] H. Weldeyesus, T. Patlatiuk, Q. Chen, C. P. Scheller, A. Yacoby, L. N. Pfeiffer, K. W. West, and D. M. Zumbühl, Supporting data for: “Edge-State Selective Measurement of Dispersions in the Quantum Hall Regime,” 10.5281/ZENODO.15863807 (2025).